Flexible Power Control of Distributed Grid-Connected Series-Photovoltaic-Battery Systems

Pan, Yiwei; Sangwongwanich, Ariya; Yang, Yongheng; Blaabjerg, Frede

Published in:
2021 IEEE Applied Power Electronics Conference and Exposition (APEC)

DOI (link to publication from Publisher):
10.1109/APEC42165.2021.9487321

Publication date:
2021

Document Version
Accepted author manuscript, peer reviewed version

Flexible Power Control of Distributed Grid-Connected Series-Photovoltaic-Battery Systems

Yiwei Pan*, Ariya Sangwongwanich*, Yongheng Yang+, and Frede Blaabjerg*
*Department of Energy Technology, Aalborg University, Aalborg, Denmark
+College of Electrical Engineering, Zhejiang University, Hangzhou, China
E-mails: ypa@et.aau.dk, ars@et.aau.dk, yang_yh@zju.edu.cn, fbl@et.aau.dk

***Abstract*—To enhance the power quality and stability of photovoltaic (PV) systems, energy storage elements such as batteries can be included. Among various structures of PV-battery-hybrid (PVBH) systems, the series configuration attracts much popularity. However, certain operating conditions have not previously been considered for the series PVBH system. For instance, when the electrical grid is overloaded, the power generation of the PVBH system should be regulated below a certain constraint. Moreover, when the battery state-of-charge (SoC) reaches an upper or lower limit, the battery converter may lose its capability in power buffering. To address these issues, a flexible power control approach for the grid-connected series PVBH system is proposed in this paper. With the proposed control method, the PV power variations can be compensated by the battery operation following a desired ramp-rate, and the total power can be limited to a certain level in order to avoid potential overloading. When the PV power is higher than the grid demand, the surplus PV power can either be absorbed by the battery or discarded depending on the battery SoC. Experimental results from hardware prototype have validated the effectiveness of the proposed solution.**

***Keywords*—Distributed control, power limiting control, ramp-rate control, series-connected converters, PV-battery systems.**

I. INTRODUCTION

An increasing integration of the renewable power generation has brought structural changes to the modern power distribution system, as well as some adverse impacts, e.g., voltage and frequency fluctuations and overloading of the distribution grid [1]-[4]. To avoid this issue and enhance the stability and power quality of distributed generation (DG) systems, solutions must be put forward to flexibly control the active power from DG systems. Among various solutions, one of the most commonly used solutions is to integrate the energy storage (ES) elements such as batteries with DG systems [5]-[9]. In order to integrate the distributed photovoltaic (PV) and battery systems in a more cost-effective way, series configurations have in recent years been introduced to the PV-battery-hybrid (PVBH) applications [6]-[12]. With the series structure, distributed PVs and batteries can be directly interfaced into separate DC rails of the series system without any additional boost stage. This will bring several benefits like high modularity, reduced cost and improved efficiency [13].

The series PVBH system was originally proposed in [6], and afterwards, efforts were mainly made for improving the output power control performance, a more efficient utilization of the PV and battery power, and a simpler control implementation. One typical distributed control approach for series PVBH systems is the hierarchical control developed in [10], [11], and [14], where individual *PQ* control for each cell, anti-over-modulation, schedulable active/reactive power of the system, and SoC balancing can be achieved. However, the hierarchical control highly relies on the communication between the central and local controllers, where several control variables should be real-time transmitted, leading to a low fault tolerant capability and reliability. To reduce the communication dependency, the current-/voltage-mode (CVM) control was introduced to series PVBH systems [8], [9], [15], [16]. In this case, one or several converters are centrally controlled as a current source, while the others are distributed controlled as voltage sources. Based on the CVM control, a decentralized ramp-rate control and virtual inertia control were developed for the series PVBH system in [8] and [9], respectively. In [8], one PV converter is selected as the current source, while others including the battery converter are operated as voltage sources. The battery converter detects the changing-rate of the grid line current, and compensates for the variations following a ramp-rate limit. Different from [8], in [9], all PV converters are controlled as voltage sources, while the battery converter is controlled as a current source, which regulates the virtual inertia of the entire system according to the variation of the grid frequency. However, only unity power factor (PF) operation was considered in the CVM control for series PVBH systems, which limits the grid support capability. When the PF of the system is non-unity, certain converters may suffer from overloading or even over-modulated if the reactive power is not properly distributed [12].

To overcome the above limitations, a distributed control scheme with low communication requirements was recently proposed for islanded series PVBH systems [12]. In this approach, individual active and reactive power control can be achieved with only local measurements. All converters can be self-synchronized without the grid phase angle information, even if they are generating non-identical active and reactive power. Both the over-modulation and reactive power distribution issues have been addressed, while the energy harvesting from PVs is maximized. Only a few variables with very slow dynamics need to be transmitted by low-bandwidth communication (LBC), which significantly reduces the communication requirement compared to the hierarchical control [10], [11]. Nonetheless, as the solution is developed for standalone systems, modifications are needed, in order to be applied to grid-connected PVBH systems. In addition, considering all the above, there are still certain limitations in prior-art control solutions:

1) When the battery SoC reaches its upper or lower limit, the battery system may fail to provide the power buffering. However, the battery SoC limitation has rarely been considered in previous studies on series PVBH systems. In [10], the battery SoC has been considered in the control, but it merely addresses the SoC balancing control among multiple batteries. The aforementioned issue has not been discussed.
2) To avoid overloading of the distribution grid, the power generation of the entire system should be controlled below a certain limit [1], [2]. However, this condition has been neglected in previous studies on series PVBH systems.

With the above concerns, a flexible power control approach based on the distributed control architecture in [12] is proposed for grid-connected series PVBH systems. During normal conditions, the PVBH system is operated in the ramp-rate control mode, in which the PV power variation is compensated by the battery following a desired ramp-rate. To avoid overloading the grid, the total power is regulated below a certain constant power limit. In this mode, the surplus active power can either be absorbed by the battery, or discarded if the battery SoC reaches its upper limit. The rest of this paper is organized as follows. In Section II, the proposed control is introduced. In Section III, experimental tests on a 500-W PVBH system are provided to validate the proposed control. Finally, concluding remarks are given in Section IV.

II. Proposed Flexible Control Scheme

A. PQ Decoupling Control for PV Converters

A 3-cell grid-connected series PVBH system is employed to demonstrate the proposed control method, as shown in Fig. 1, where two PV converters and one battery converter are connected in series. For n-cell systems (n is the number of series-connected converters), it is assumed that only one battery converter is used for the PVBH system in the following analysis. The PVBH system can be represented by the phasor diagram as shown in Fig. 2, where the total voltage phasor $\dot{V}_{\text{total}}$ is synthesized by the summation of the cell voltage phasors $\dot{V}_1$, $\dot{V}_2$ and $\dot{V}_3$ (the voltage phasors of converter #1, #2, and #3). According to Fig. 2, the increase on the amplitude of $\dot{V}_1$ will lead to an increase of both active and reactive power of converter #1, while the increase of the PF angle θ_1 will result in a decrease of the active power and increase of the reactive power. According to [12], the output power variations for the k^{th} converter can be obtained as

$$\begin{bmatrix}\Delta P_{\text{k}}\\ \Delta Q_{\text{k}}\end{bmatrix}=I_{\text{g}}\begin{bmatrix}\cos\theta_{\text{k}} & -V_{\text{k}}\sin\theta_{\text{k}}\\ \sin\theta_{\text{k}} & V_{\text{k}}\cos\theta_{\text{k}}\end{bmatrix}\begin{bmatrix}\Delta V_{\text{k}}\\ \Delta\theta_{\text{k}}\end{bmatrix}=I_{\text{g}}\boldsymbol{A}\begin{bmatrix}\Delta V_{\text{k}}\\ \Delta\theta_{\text{k}}\end{bmatrix} \tag{1}$$

where V_{k} and θ_{k} are the AC voltage amplitude and PF angle of the k^{th} converter, respectively, ΔP_{k}, ΔQ_{k}, ΔV_{k} and $\Delta\theta_{\text{k}}$ are the increments of the active power, reactive power, voltage amplitude and PF angle of the k^{th} converter, respectively, and $\boldsymbol{A}$ is the coupling matrix. From (1), it is known that there is a PF angle-dependent coupling relationship between ΔP_{k}, ΔQ_{k} and ΔV_{k}, $\Delta\theta_{\text{k}}$, which should be decoupled. By solving the inverse matrix of A, it gives

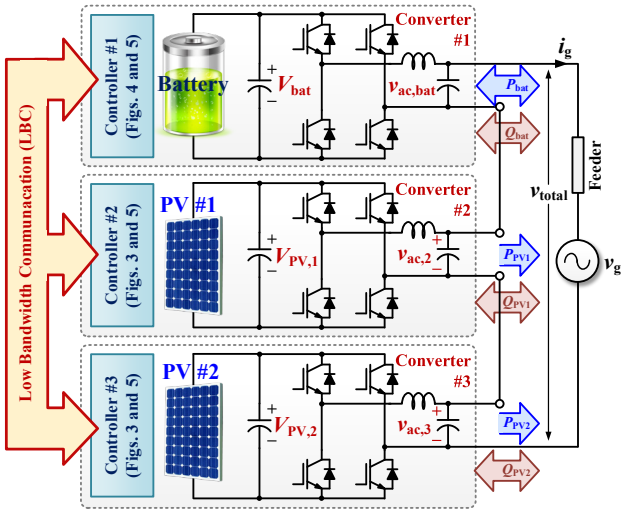

Fig. 1. Hardware schematic of a 3-cell series PVBH system, where $v_{\text{ac,k}}$ and $v_{\text{ac,bat}}$ are the AC voltages of the k^{th} converter cell and the battery cell, respectively, $V_{\text{PV,m}}$ and V_{bat} are the DC voltages of PV #m and the battery, respectively, and v_{total}, v_{g} and i_{g} are the total output AC voltage, grid voltage and grid current of the system, respectively.

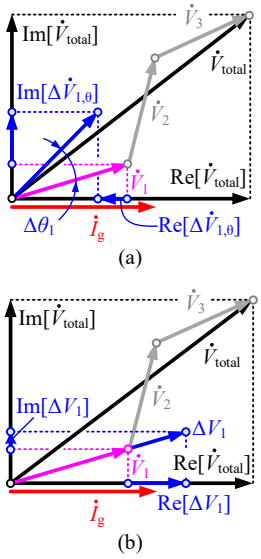

Fig. 2. Phasor diagrams of the 3-cell series system when (a) the phase angle of converter #1 varies, and (b) when the output voltage amplitude of converter #1 varies. Re[·] and Im[·] denote the real and imaginary part of the phasor, respectively.

$$\begin{bmatrix}\Delta V_{\text{k}}\\ \Delta\theta_{\text{k}}\end{bmatrix}=\frac{\boldsymbol{A}^{-1}}{I_{\text{g}}}\begin{bmatrix}\Delta P_{\text{k}}\\ \Delta Q_{\text{k}}\end{bmatrix}=\frac{1}{I_{\text{g}}}\begin{bmatrix}\cos\theta_{\text{k}} & \sin\theta_{\text{k}}\\ -\dfrac{\sin\theta_{\text{k}}}{V_{\text{k}}} & \dfrac{\cos\theta_{\text{k}}}{V_{\text{k}}}\end{bmatrix}\begin{bmatrix}\Delta P_{\text{k}}\\ \Delta Q_{\text{k}}\end{bmatrix}. \tag{2}$$

Considering $\Delta\theta_{\text{k}}=(1/s)\cdot\Delta\omega_{\text{k}}$, where $\Delta\omega_{\text{k}}$ is the increment on the angular frequency of the k^{th} converter, and $\Delta\theta_{\text{k}}$ can be controlled by regulating $\Delta\omega_{\text{k}}$. Then, according to (2), a PQ decoupling control scheme can be obtained, as shown in Fig. 3 [12]. Both the active and reactive power of the PV converter are regulated by proportional-integral (PI) controllers, with their outputs being decoupled by the decoupling matrix. Then, the increments on the amplitude and angular frequency can be calculated. The active power

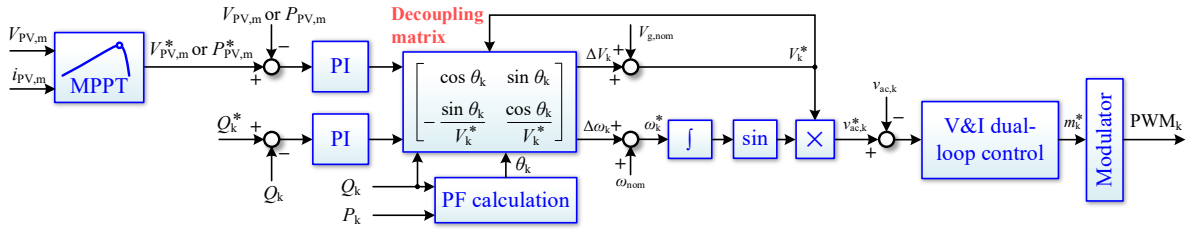

Fig. 3. Control diagram of the PV converter, where $V_{PV,m}$ denotes the DC voltage of PV #m, $P_{PV,m}$ denotes the active power for the converter with PV #m, Q_k denotes the reactive power of the k^{th} converter, m_k^* is the modulation index, and PWM_k refers to the PWM signal for the k^{th} converter.

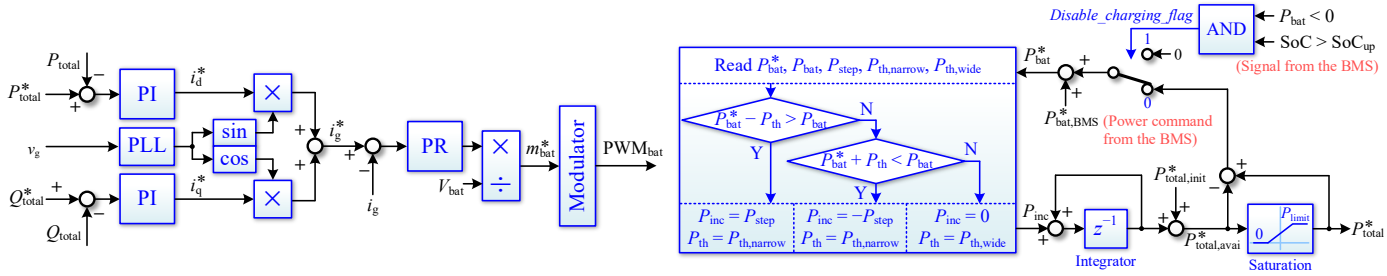

Fig. 4. Control diagram of the battery converter: (a) power loops and the current loop, and (b) the ramp-rate control and the power limiting control scheme, where PWM_{bat} refers to the PWM signal for the battery converter, $P^*_{total,init}$ and $P^*_{total,avai}$ are the initial total power reference and the reference of the total available power, respectively, P_{step} is the step-size of the power increment within one control cycle, BMS is the acronym for the battery management system.

reference can be obtained by the maximum power point tracking (MPPT) control, being either the PV voltage reference $V^*_{PV,m}$ or PV power reference $P^*_{PV,m}$. The output voltage reference of the k^{th} converter $V_{ac,k}$ is then calculated by

$$v^*_{ac,k} = V^*_k \sin\left(\int \omega^*_k \mathrm{d}t\right) = \left(\frac{V_{g,nom}}{n} + \Delta V_k\right) \sin\left(\int (\omega_{nom} + \Delta\omega_k)\, \mathrm{d}t\right) \quad (7)$$

where $V_{g,nom}$ and ω_{nom} are the nominal amplitude and frequency of the grid voltage, respectively. Then, through the voltage and current dual-loop control, individual power control can be achieved with only local measurements for the PV converters, as shown in Fig. 3.

B. Control of the Battery Converter

The power control diagram of the battery converter is shown in Fig. 4(a), where the total active and reactive power references, denoted as P^*_{total} and Q^*_{total}, are regulated by PI controllers, which generate the grid current references under the *dq*-frame (i^*_d and i^*_q). Then, with the grid voltage phase-angle θ_g being calculated by a phase-locked loop (PLL), the grid current reference i^*_g can be obtained, which is regulated by a proportional-resonant (PR) controller, and the modulation index for the battery converter (m^*_{bat}) can thus be calculated.

C. Flexible Control Method

The control diagram of the proposed flexible power control for the series PVBH system is shown in Fig. 4(b). The system can be operated in three modes:

1) *Mode 1: Normal operation mode (ramp-rate control mode).* As shown in Fig. 4(b), if the reference of the total available power $P^*_{total,avai}$ is below the power limit while the battery SoC is within the normal operational range, the battery converter compensates for the PV power variation and regulates the variation of the total power following a desired ramp-rate. Here, the normal operational range of the battery is defined as the battery SoC being within the range of (SoC_{dw}, SoC_{up}), where SoC_{dw} and SoC_{up} are the lower and upper thresholds of the battery SoC. They can be selected as 20% and 80% in practice [5]. The power reference for the battery $P^*_{bat,BMS}$ is provided by the battery management system (BMS), which can be set as zero by default (neither charge nor discharge). If the measured battery power is higher than $P^*_{bat} + P_{th}$, or lower than $P^*_{bat} - P_{th}$, the reference of the total available power $P^*_{total,avai}$ will be decreased or increased by P_{inc} within a control period, respectively. Here, P_{th} is a small threshold to avoid disturbance on the power reference in steady-state. By doing so, when the variation of PV power is small, the total power will not be affected, and the small power variation will be compensated by the battery. When the PV power variation becomes larger, the total power reference will gradually approach a new steady-state value with a ramp-rate of P_{inc} / T_s (T_s refers to the control period), until the active power of the battery cell is approximately zero again (within the range between $P^*_{bat} - P_{th}$ and $P^*_{bat} + P_{th}$). To improve the control perform-ance, two comparison thresholds are assigned to P_{th} in different cases, with the larger threshold being $P_{th,wide}$, and the smaller one being $P_{th,narrow}$. When the control enters into the steady-state, i.e., $P^*_{bat} - P_{th} < P_{bat} < P^*_{bat} + P_{th}$, P_{th} is set to be larger as $P_{th,wide}$ to avoid frequent variation on the power reference. On the other hand, when the battery power is beyond the range of $\left(P^*_{bat} - P_{th}, P^*_{bat} + P_{th}\right)$, which means the control is in the dynamic zone, $P_{th,narrow}$ is assigned to P_{th}, in order to alleviate the steady-state battery power control errors induced by P_{th}.
2) *Mode 2: Power limiting control (PLC) mode with battery charging enabled.* As shown in Fig. 4(b),

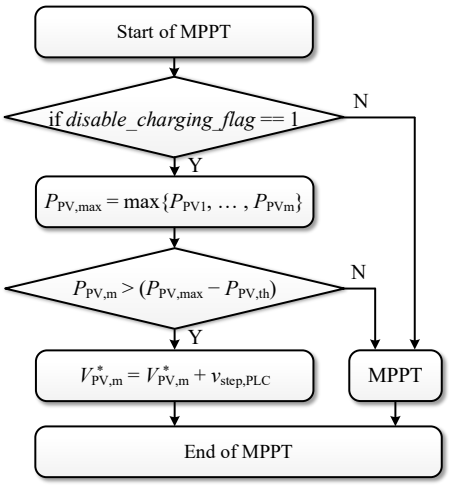

Fig. 5. Modified MPPT algorithm in power limiting mode with battery charging disabled.

if $P^*_{total,avai}$ is higher than the power limit P_{limit}, while the battery SoC is lower than SoC_{up}, the total active power reference P^*_{total} will be limited to P_{limit}, and the *Disable_charging_flag* will be set to zero, as shown in Fig. 4(b). Then, $\left(P^*_{total} - P^*_{total,avai}\right)$ will be set as the power reference of the battery converter, and the surplus power will be absorbed by the battery.

3) *Mode 3: PLC mode with battery charging disabled.* If $P^*_{total,avai}$ is higher than P_{limit}, while the battery SoC is higher than SoC_{up}, the surplus power will be directly discarded to avoid overcharging of the battery. As shown in Fig. 4(b), the *Disable_charging_flag* will be set as 1, and the battery power reference is thus kept constant at 0. Then, as shown in Fig. 5, if the power of the m^{th} PV is larger than ($P_{PV,max} - P_{PV,th}$), the DC voltage reference for the m^{th} PV is increased by $v_{step,PLC}$ to discard a part of PV power. Here, $P_{PV,max}$ is the maximum power of all PV converters, $P_{PV,th}$ is a threshold value, and $v_{step,PLC}$ is the perturbation step-size of the PLC strategy. The power limiting command is sent from the battery converter to PV converters through the LBC. By doing so, in steady state, the PV voltages will oscillate around a voltage higher than the maximum power point (MPP) voltage, while the power of the battery converter is kept approximately zero.

In addition, when the battery SoC reaches its upper or lower limit, the battery converter can be operated in the discharging mode or charging mode, respectively, by setting the value of $P^*_{bat,BMS}$. In this way, the battery SoC can be maintained in the normal operation range.

D. Reactive Power Distribution and Anti-Over-Modulation (AOM) Control

The reactive power distribution among the series converters and the anti-over-modulation control of individual converters are two essential issues for series PVBH systems [12]. Since the analysis and control methods to address both issues have been presented in [12], they will not be detailed in this paper. The reactive power distribution strategy and the anti-over-modulation loops in [12] are directly applied to the grid-connected PVBH system.

TABLE I
EXPERIMENTAL PARAMETERS.

Circuit parameters	Value
PV rated power per panel	290 W
DC link capacitor for PV converters	2000 μF
DC link capacitor for the battery converter	680 μF
Output LC filter of each converter	1.8 mH / 30 μF
Nominal voltage of the battery	48 V
Amplitude of the nominal grid voltage $V_{g,nom}$	78 V
Control parameters	**Value**
Switching frequency	10 kHz
Controller sampling frequency	10 kHz
MPPT sampling rate	5 Hz
MPPT step-size	2.5 V
Increment for the ramp-rate control	P_{step} = 0.02 W,
Power limiting value	P_{limit} = 400 W
Thresholds for the battery power control	$P_{th,narrow}$ = 5 W, $P_{th,wide}$ = 10 W
Threshold for the PLC with battery charging disabled	$P_{PV,th}$ = 10 W
Reactive power distribution coefficient [12]	h = 2.8
Upper threshold for AOM loops [12]	$m_{th,H}$ = 0.9
Lower threshold for AOM loops [12]	$m_{th,L}$ = 0.8
Perturbation step-size of the PLC	$V_{step,PLC}$ = 1.2 V
Power control parameters for PV converters[a]	$k_{p,p} = -2$, $k_{i,p} = -2$, $k_{p,q} = 0.12$, $k_{i,q} = 0.4$
Power control parameters for the battery converter[b]	$k_{p,p,total} = k_{p,q,total} = 0.005$, $k_{i,p,total} = k_{i,q,total} = 1$
Communication baud rate	9600 bps

[a]The active power control of PV converters is realized by controlling the PV voltages. $k_{p,p}$, $k_{i,p}$, $k_{p,q}$, and $k_{i,q}$ are the proportional and integral gains for the active and reactive power control, correspondingly.
[b]$k_{p,p,total}$, $k_{i,p,total}$, $k_{p,q,total}$ and $k_{i,q,total}$ are the proportional and integral gains for the active and reactive power control loops in the battery converter, correspondingly.

III. EXPERIMENTAL VALIDATION

To validate the effectiveness of the proposed control, experiments have been performed on a down-scaled 3-cell series PVBH system, which is assembled with three Infineon FS50R12KT4_B15 IGBT modules. One Keysight E4360A PV simulator was used to emulate the two PV modules, and one Delta Elektronika SM330 DC power supply in parallel with a resistor bank was adopted to mimic the battery. Three TMS320F28335 digital signal processors were employed as individual controllers, which are interlinked with the RS-485 serial communication. The parameters of the PVBH system are shown in Table I.

Case 1: The ramp-up and the power limiting control performance are shown in Figs. 6 and 7 (Mode 1 and 2), where PV #1 is operating at 47% rated power, while PV #2 is operating at 100% rated power in the initial stage. As shown in Fig. 7, the DC voltage of PV #1 is oscillating around 55 V, being the voltage of its MPP, and approximately 110-W power is provided by the 1st PV converter. Since the power for the two PVs are severely unbalanced, the power of PV #2 is also limited to avoid over-modulation, being about 140 W in the

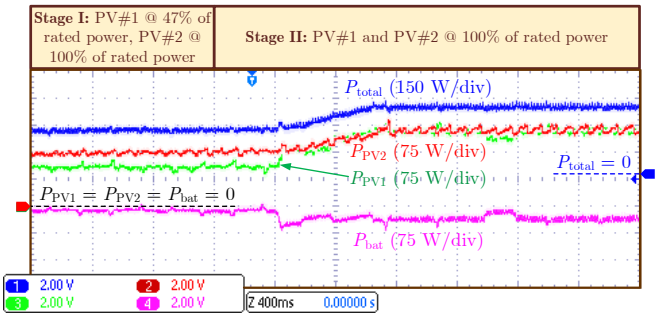

Fig. 6. Power limiting control performance when battery charging is permitted (time [400 ms/div]).

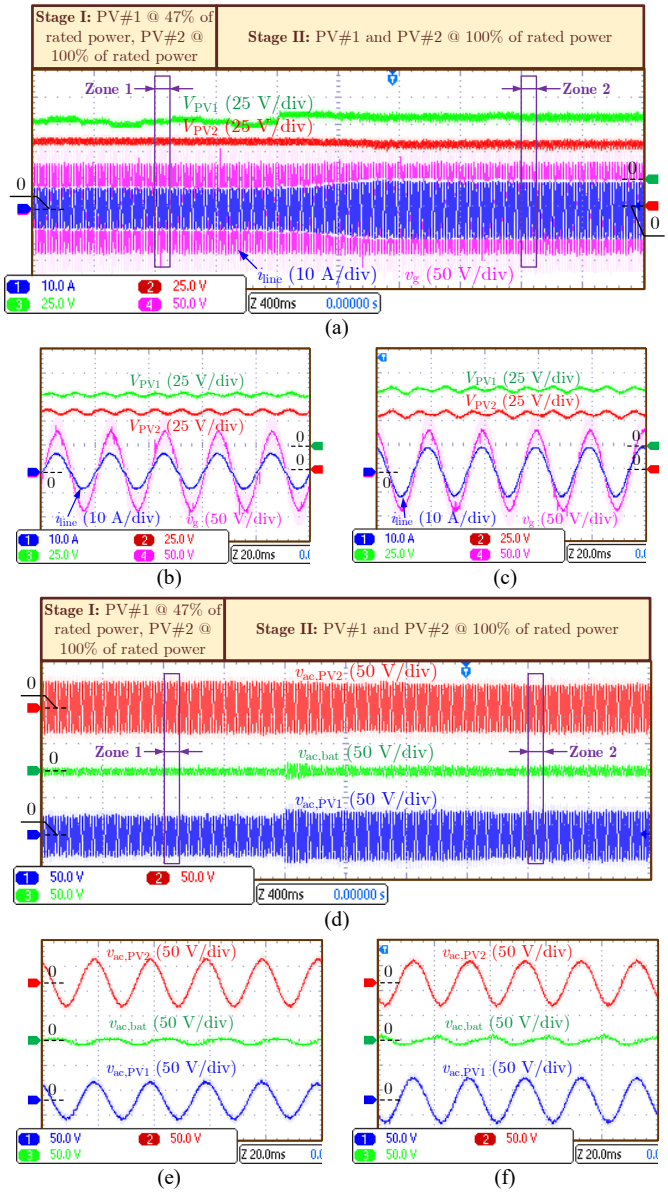

Fig. 7. Current and voltage responses of the system under PLC while the battery charging is permitted (the time scale is 400 ms/div for Figs. 7(a) and (d), and 20 ms/div for Figs. 7(b), (c), (e) and (f)): (a) PV voltages, grid voltage and current, (b) zoomed-in plot of Zone 1 in Fig. 7(a), (c) zoomed-in plot of Zone 2 in Fig. 7(a), (d) output voltages of the three converters, (e) zoomed-in plot of Zone 1 in Figs. 7(d), and (f) zoomed-in plot of Zone 2 in Fig. 7(d).

initial stage. After the step change of the PV power, P_{total} slowly increases following a ramp-rate of 200 W/s, while P_{PV1} increases quickly at the beginning, and then ramps up together with P_{PV2}. The reason why P_{PV1} and P_{PV2} do not reach the 100% of their rated power immediately is the over-modulation, which can be confirmed by Fig. 7(d). As shown in Fig. 7(d), the amplitude of the output voltage for the first PV converter is about 50 V, while the DC voltage of PV #1 is 60 V (see Fig. 7(a)). The amplitude of the modulation index for the first PV converter can thus be estimated as 0.83, which is within the dead-band of the AOM control, as shown in Table I. In steady state, due to the PLC, P_{total} is saturated when it reaches 400 W, and the battery is charged in order to absorb the surplus active power. The power from each PV converter is about 220 W, with a part of the power being discarded to prevent from over-modulation, as shown in Fig. 7(f), where the two PV converters are generating their maximum AC voltages. Therefore, the power-limiting capability can be achieved with the proposed control, and a part of the PV power can be stored in the battery to utilize as much PV power as possible.

Case 2: The ramp-down control performance (Mode 1) is demonstrated in Figs. 8 and 9. In the initial stage, both PV #1 and #2 are operating at 70% rated power. In the beginning, approximately 180-W active power is provided by each PV converter, and almost no power from the battery converter. Then, the power of PV #2 suddenly decreases to 35% of its rated power, as shown in Fig. 8, where the power of PV #2 decreases abruptly to 80 W, while PV #1 keeps operating at 75% of its rated power. As shown in Figs. 8 and 9(a), the envelope of the grid current slowly decreases, as well as the total active power, which enters into the steady-state in 0.8 seconds after the PV power change. The steady-state total power is around 190 W. It can thus be obtained that the total power decreases with a ramp-rate of −200 W/s. In steady state, PV #2 is operating at its MPP, as shown in Fig. 9(a), where V_{PV2} oscillates around 55 V. Due to the reduction of the grid current, P_{PV1} also slowly decreases to 120 W. It can be noticed that the amplitude of $v_{ac,PV2}$ is within the dead-band of the AOM control, and as a result, about 60-W active power needs to be discarded to avoid the over-modulation. In both the initial stage and steady state, almost no power is provided by the battery, as shown in Fig. 8, while during the dynamics, the battery converter provides the active power support for 800-ms, with its peak power being about 100 W. The grid current is kept sinusoidal during the entire operation.

Case 3: To demonstrate the control performance of the system under the PLC with different SoC status (Mode 3), experimental results are shown in Fig. 10. The initial condition is the same with the steady-state condition of Case 3, and the *Disable_charging_flag* is enabled due to a high SoC. As a result, the power of the battery converter quickly rises and oscillates around zero, after the enabling of the command. Consequently, P_{PV1} and P_{PV2} oscillate around 200 W in steady state. Since only a small amount of power is discarded by each PV converter, there are no obvious variations on the PV voltages. The total power and the grid current are kept constant during the entire process.

Moreover, if the charging of the battery is permitted again, *Disable_charging_flag* will be reset as 0. Experimental results

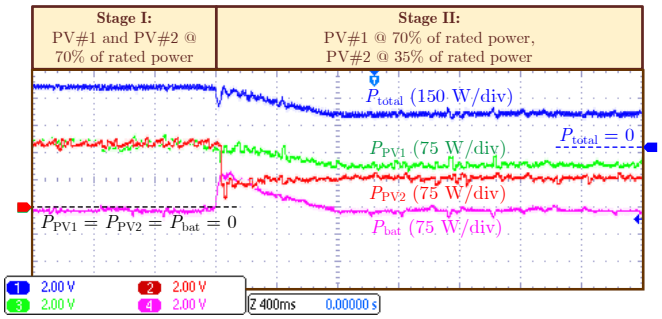

Fig. 8. Power ramp-down control performance of the system when the PV power decreases (time [400 ms/div]).

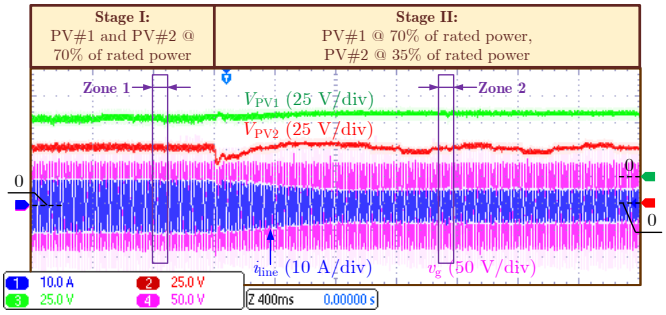

(a)

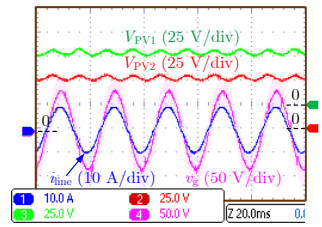

(b)

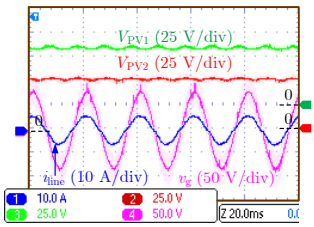

(c)

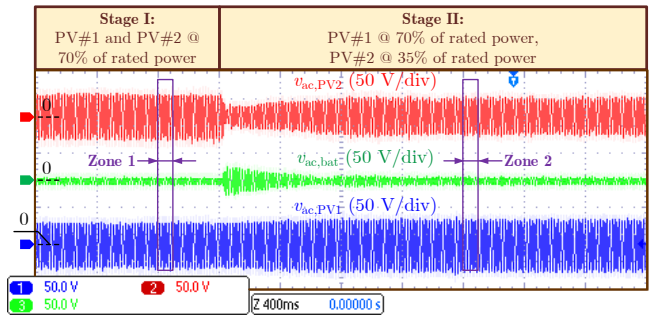

(d)

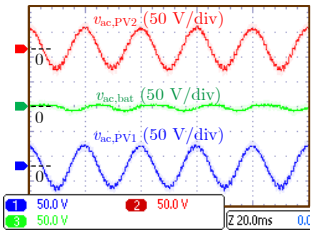

(e)

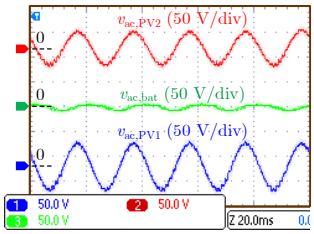

(f)

Fig. 9. Current and voltage responses of the system when the PV power decreases (the time scale is 400 ms/div for Figs. 9(a) and (d), and 20 ms/div for Figs. 9(b), (c), (e) and (f)): (a) PV voltages, grid voltage and current, (b) zoomed-in plot of Zone 1 in Fig. 9(a), (c) zoomed-in plot of Zone 2 in Fig. 9(a), (d) output voltages of the three converters, (e) zoomed-in plot of Zone 1 in Fig. 9(d), and (f) zoomed-in plot of Zone 2 in Fig. 9(d).

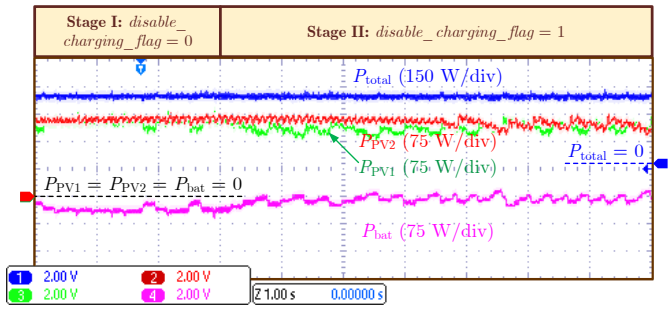

(a)

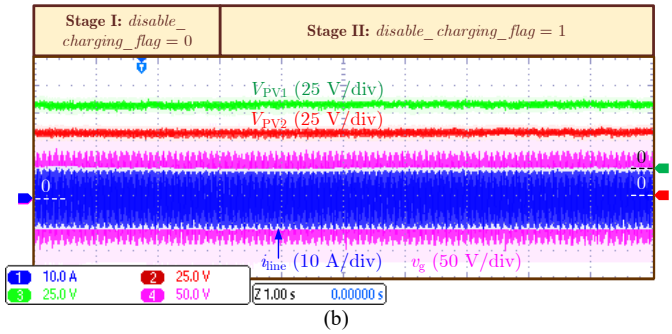

(b)

Fig. 10. Performance of the system under power limiting control and when the battery charging is disabled (time [1 s/div]): (a) total active power and the active power of each converter, and (b) PV voltages, grid voltage and current.

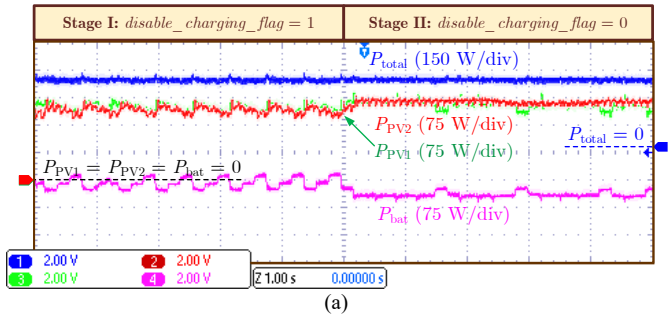

(a)

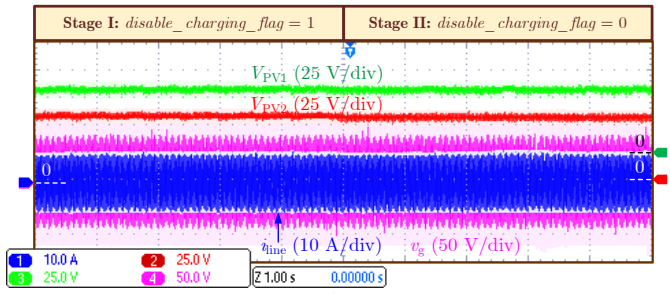

(b)

Fig. 11. Performance of the system under PLC and when the battery charging is again enabled (time [1 s/div]): (a) total active power and the active power of each converter, and (b) PV voltages, grid voltage and current.

are shown in Fig. 11 to demonstrate the performance when the *Disable_charging_flag* switches from 1 to 0 (switch from Mode 3 to Mode 2). The initial state of this test is the same with the steady state conditions in Fig. 10. As shown in Fig. 11(a), after the reset, the battery starts to charge at 40 W again, and the power from each PV converter rises back to 220 W. The total power, as well as the grid current, are not affected by the battery power control, as shown in Fig. 11.

Case 4: Finally, experimental results are provided in Figs. 12 and 13 when the PF of the system becomes non-unity. In the initial stage, the test condition is the same with the steady state of Case 1. Then, the total reactive power reference ramps up to 200 Var. As it can be seen from Fig. 12, since the reactive power will slightly increase the amplitude of the grid current, the power from the each PV converters is also increased a bit, being 230 W in steady state. Consequently, the battery is charged at a higher power, which is around −60 W. Since the amount of active power from the battery converter is much less than the PV converters, all reactive power is supported by the battery converter, as it can be observed from Fig. 12, where the reactive power of the battery converter slowly increases to 200 Var, while the reactive power is kept zero for the two PV converters [12]. The reactive power distribution performance can be further confirmed by Fig. 13(f), where $v_{ac,PV1}$ and $v_{ac,PV2}$ are in phase, while $v_{ac,bat}$ has the minimum amplitude, and is phase-shifted compared with $v_{ac,PV1}$ and $v_{ac,PV2}$. During the entire process, the grid current is kept stable with a high power quality.

IV. Conclusions

A flexible power control method for grid-connected series PVBH systems was proposed in this paper. Based on a *PQ* decoupling control, the proposed control can be realized with very low communication requirements, which is very suitable for distributed systems. With the proposed control strategy, energy harvesting from PV modules can be maximized, while the PV power variation is compensated by the battery following a desired ramp-rate, which will enhance the stability and power quality of DG systems. To prevent the network from overloading, the total active power can also be regulated under a certain limit. In this operating mode, the surplus active power can either be absorbed by the battery, or discarded if the battery SoC reaches its upper limit. Moreover, the battery SoC can also be self-balanced according the power command from the BMS. Experimental results from the hardware prototype have validated the effectiveness of the proposed control solution in terms of the ramp-rate control and the PLC control under different battery SoC status.

References

[1] Y. Yang, K. A. Kim, F. Blaabjerg, and A. Sangwongwanich, *Advances in Grid-Connected Photovoltaic Power Conversion Systems*, Publisher: Woodhead Publishing, 2018.

[2] H. D. Tafti, A. Sangwongwanich, Y. Yang, J. Pou, G. Konstantinou, and F. Blaabjerg, "An adaptive control scheme for flexible power point tracking in photovoltaic systems," *IEEE Trans. Power Electron.*, vol. 34, no. 6, pp. 5451-5463, Jun. 2019.

[3] A. Sangwongwanich, Y. Yang, F. Blaabjerg, and H. Wang, "Benchmarking of constant power generation strategies for single-phase grid-connected photovoltaic systems," *IEEE Trans. Ind. Appl.*, vol. 54, no. 1, pp. 447-457, Jan.-Feb. 2018.

[4] H. D. Tafti, G. Konstantinou, J. E. Fletcher, G. G. Farivar, S. Ceballos, J. Pou, and C. D. Townsend, "Flexible power point tracking in cascaded H-bridge converter-based photovoltaic systems," in *Proc. 46th Annu. Conf. IEEE Ind. Electron. Soc.*, Oct. 2020, pp. 1826-1830.

[5] S. Adhikari and F. Li, "Coordinated V-f and P-Q control of solar photovoltaic generators with MPPT and battery storage in microgrids," *IEEE Trans. Smart Grid*, vol. 5, no. 3, pp. 1270-1281, May 2014.

[6] L. Liu, H. Li, Z. Wu, and Y. Zhou, "A cascaded photovoltaic system integrating segmented energy storages with self-regulating power allocation control and wide range reactive power compensation," *IEEE Trans. Power Electron.*, vol. 26, no. 12, pp. 3545-3559, Dec. 2011.

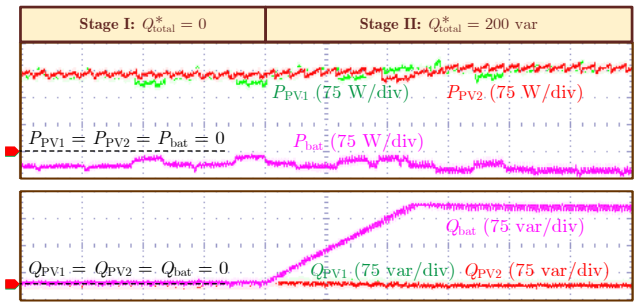

Fig. 12. Power control performance of the system with reactive power injection (time [400 ms/div]).

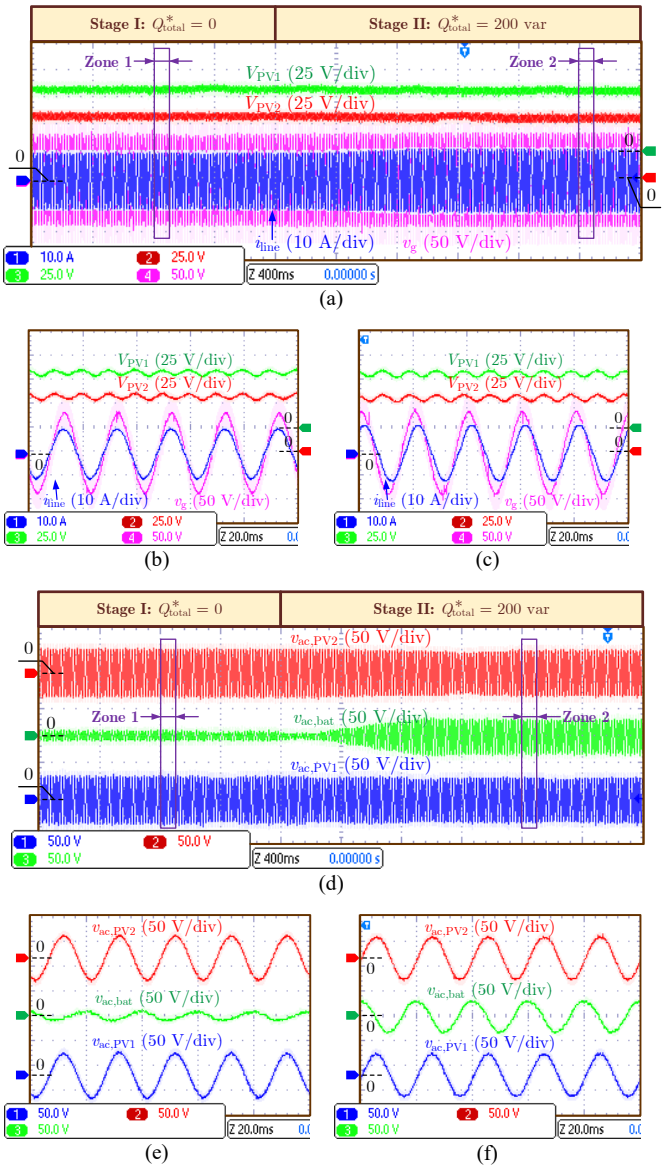

Fig. 13. Current and voltage responses of the system with reactive power injection (the time scale is 400 ms/div for Figs. 13(a) and (d), and 20 ms/div for Figs. 13(b), (c), (e) and (f)): (a) PV voltages, grid voltage and current, (b) zoomed-in plot of Zone 1 in Fig. 13(a), (c) zoomed-in plot of Zone 2 in Fig. 13(a), (d) output voltages of the three converters, (e) zoomed-in plot of Zone 1 in Figs. 13(d), and (f) zoomed-in plot of Zone 2 in Fig. 13(d).

[7] A. Marquez, J. I. Leon, S. Vazquez, L. G. Franquelo, and S. Kouro, "Operation of an hybrid PV-battery system with improved harmonic performance," in *Proc. 43rd Annu. Conf. IEEE Ind. Electron. Soc*., 2017, pp. 4272–4277.

[8] N. Kim and B. Parkhideh, "Control and operating range analysis of an AC-stacked PV inverter architecture integrated with a battery," *IEEE Trans. Power Electron*., vol. 33, no. 12, pp. 10032-10037, Dec. 2018.

[9] H. Liao, X. Zhang, and X. Hou, "A decentralized control of series-connected PV-ES inverters with MPPT and virtual inertia functionality," in *Proc. IEEE APEC*, Mar. 2020, pp. 3221-3224.

[10] Y. Pan, C. Zhang, S. Yuan, A. Chen, and J. He, "A decentralized control method for series connected PV battery hybrid microgrid," in *Proc. IEEE ITEC Asia-Pacific*, Aug. 2017, pp. 1–6.

[11] Q. Zhang and K. Sun, "A flexible power control for PV-battery hybrid system using cascaded H-bridge converters," *IEEE J. Emerg. Sel. Topi. Power Electron*., vol. 7, no. 4, pp. 2184-2195, Dec. 2019.

[12] Y. Pan, A. Sangwongwanich, Y. Yang, and F. Blaabjerg, "Distributed control of islanded series PV-battery-hybrid systems with low communication burden," *IEEE Trans. Power Electron.*, DOI: 10.1109/TPEL.2021.3063111.

[13] Y. Pan, A. Sangwongwanich, Y. Yang, and F. Blaabjerg, "A phase-shifting MPPT to mitigate interharmonics from cascaded H-bridge PV inverters," *IEEE Trans. Ind. Appl*., DOI: 10.1109/TIA.2020.3000969.

[14] J. He, Y. Li, C. Wang, Y. Pan, C. Zhang, and X. Xing, "Hybrid microgrid with parallel- and series-connected microconverters," *IEEE Trans. Power Electron*., vol. 33, no. 6, pp. 4817-4831, June 2018.

[15] H. Jafarian, S. Bhowmik, and B. Parkhideh, "Hybrid current-/voltage-mode control scheme for distributed AC-stacked PV inverter with low-bandwidth communication requirements," *IEEE Trans. Ind. Electron.*, vol. 65, no. 1, pp. 321-330, Jan. 2018.

[16] P.-H. Wu, Y.-C. Su, J.-L. Shie, and P.-T. Cheng, "A distributed control technique for the multilevel cascaded converter," *IEEE Trans. Ind. Appl*., vol. 55, no. 2, pp. 1649-1657, Mar.-Apr. 2019.